

Electronic Supplementary Information

Interpretation of Mott-Schottky Plots of Photoanodes for Water Splitting

Sandheep Ravishankar^{1*}, Juan Bisquert² and Thomas Kirchartz^{1,3}

¹IEK-5 Photovoltaik, Forschungszentrum Jülich, 52425 Jülich, Germany

²Institute of Advanced Materials, Universitat Jaume I, Castellón de la Plana 12071, Spain

³Faculty of Engineering and CENIDE, University of Duisburg-Essen, Carl-Benz-Str. 199, 47057 Duisburg, Germany

A1 Drift-diffusion Simulations

All simulations were carried out using SCAPS – a Solar Cell Capacitance Simulator,¹ which numerically solves three coupled differential equations in one dimension. These differential equations are the Poisson equation

$$\frac{\partial^2 \phi}{\partial x^2} = -\frac{\rho}{\varepsilon}, \quad (\text{S1})$$

where the space charge density is given by $\rho = q(p - n - N_A + N_D)$, where n and p are the densities of electrons and holes, N_A is the density of ionized acceptor-like defects and N_D the density of ionized donor-like defects. At steady state ($dn/dt = 0$ and $dp/dt = 0$), the continuity equations are given by

$$-\frac{1}{q} \frac{dJ_n(x)}{dx} = -D_n \frac{d^2 n(x)}{dx^2} - F\mu_n \frac{dn(x)}{dx} = G(x) - R(x, n, p) \quad (\text{S2})$$

for electrons and

$$\frac{1}{q} \frac{dJ_p(x)}{dx} = -D_p \frac{d^2 p(x)}{dx^2} + F\mu_p \frac{dp(x)}{dx} = G(x) - R(x, n, p) \quad (\text{S3})$$

for holes. In equations S2 and S3, $D_{n,p} = kT\mu_{n,p}/q$ are the diffusion coefficients for electrons and holes, $\mu_{n,p}$ are the mobilities of electrons and holes, R is the recombination rate, G is the generation rate and F is the electric field. Equations S1 to S3 are numerically solved using suitable boundary conditions for each differential equation. The electrolyte was modelled as a metallic contact whose Fermi level corresponds to the water oxidation potential (+1.23 V vs RHE). The electron and hole currents at the respective interfaces with the collecting contact and electrolyte are modelled using the equation

$$j = k(n - n_0), \quad (\text{S4})$$

where k is a charge transfer velocity and n and n_0 are the non-equilibrium and equilibrium electron/hole densities respectively. The slow kinetics of holes at the photoanode/electrolyte interface was thus modelled by choosing a low value of k for the holes at this interface (see table S1, S2 and S3). The voltage was applied to the electron contact. Further information on drift-diffusion simulations can be found in references²⁻⁴.

Table S1 Parameters used for the SCAPS simulations in figure 1.

parameter	electron contact	photoanode (Bismuth Vanadate)	electrolyte
thickness (nm)		500 nm	
relative permittivity		68	
bandgap (eV)		2.4	
electron affinity (eV)		4.15	
effective DOS CB (cm ⁻³)		2×10^{18}	
effective DOS VB (cm ⁻³)		2×10^{18}	
radiative recombination coefficient (cm ³ /s)		6×10^{-11}	
injection barrier (eV)	0.05		1.05
electron mobility (cm ² /Vs)		0.02	
hole mobility (cm ² /Vs)		0.02	
doping density (cm ⁻³)		3×10^{17}	
workfunction (eV)	4.2		5.5
electron charge transfer velocity (cm/s)	10^7		10^{10}
hole charge transfer velocity (cm/s)	10^{10}		10^1

Table S2 Parameters used for the SCAPS simulations in figure 2.

parameter	electron contact	photoanode (Bismuth Vanadate)	electrolyte
thickness (nm)		500 nm	
relative permittivity		68	
bandgap (eV)		2.4	
electron affinity (eV)		4.15	
effective DOS CB (cm ⁻³)		2×10^{18}	
effective DOS VB (cm ⁻³)		2×10^{18}	
radiative recombination coefficient (cm ³ /s)		6×10^{-11}	
injection barrier (eV)	0.05		1.05
electron mobility (cm ² /Vs)		0.02	
hole mobility (cm ² /Vs)		0.02	
doping density (cm ⁻³)		5×10^{17}	
workfunction (eV)	4.2		5.5
electron charge transfer velocity (cm/s)	10^7		10^{10}
hole charge transfer velocity (cm/s)	10^{10}		10^1

Table S3 Parameters used for the SCAPS simulations in figure 3.

parameter	electron contact	photoanode (Bismuth Vanadate)	electrolyte
thickness (nm)		500 nm	
relative permittivity		68	
bandgap (eV)		2.4	
electron affinity (eV)		4.15	
effective DOS CB (cm^{-3})		2×10^{18}	
effective DOS VB (cm^{-3})		2×10^{18}	
radiative recombination coefficient (cm^3/s)		6×10^{-11}	
injection barrier (eV)	0.05		1.05
electron mobility (cm^2/Vs)		0.02	
hole mobility (cm^2/Vs)		0.02	
doping density (cm^{-3})		0	
workfunction (eV)	4.2		5.5
electron charge transfer velocity (cm/s)	10^7		10^{10}
hole charge transfer velocity (cm/s)	10^{10}		10^1

A2 Discussion of the parameters

Bandgap: Since a BiVO_4 photoanode was considered, the bandgap was chosen from ref.⁵.

Relative permittivity: The relative permittivity of BiVO_4 was chosen from ref.⁶.

Electron affinity and injection barriers: The electron affinity was chosen based on the workfunction of the metal contact, to make a small injection barrier for the electrons at the electron contact. The hole injection barrier (distance between valence band and water oxidation redox level) was chosen from ref.⁷.

Density of states: The density of states was chosen arbitrarily.

Radiative recombination coefficient: The radiative recombination coefficient was chosen arbitrarily.

Workfunction: The electron contact was assumed to be Ag and hence, a workfunction of 4.2 eV was chosen. The energetic distance of the water oxidation redox level to surface vacuum level was chosen based on ref.⁷.

Mobility: The electron mobility was reduced by one order from that reported in ref.⁸ to account for the fact that we consider an undoped BiVO_4 photoanode. We assumed electron and hole mobilities to be the same for simplicity. For the doped BiVO_4 simulations, we assume that the mobilities remain the same as that of the undoped case for simplicity.

Charge transfer velocities: For the electron and hole transfer rates, we assume that the interfaces are blocking for the opposite carrier. This means that all the excess holes at the

electron contact/photoanode interface recombine and are lost, and all the excess electrons at the photoanode/electrolyte interface recombine and are lost. Thus, the charge transfer velocity for holes at the electron-contact/photoanode interface and for electrons at the photoanode/electrolyte interface was set very high, to a value of 10^{10} cm/s. We also assumed that the metal contact is a good extractor of electrons and hence set the electron charge transfer velocity at this interface to 10^7 cm/s. For the hole transfer velocity from the photoanode to the electrolyte, we set the value very low – to 10^1 cm/s to account for the slow kinetics of hole transfer.⁹⁻¹² While the value itself is not obtained from literature, it was chosen demonstratively to simulate the band diagram under such a condition of slow hole transfer.

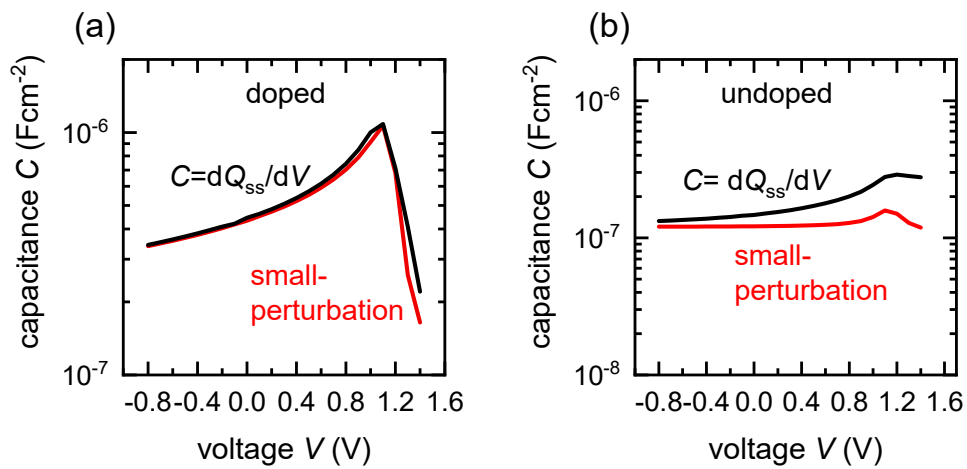


Figure S1 Capacitance calculated from SCAPS simulations using two methods – from a small-perturbation of voltage (small-perturbation) and from the ratio of the differential of the average net charge density Q_{ss} in the photoanode at steady-state and the differential voltage. The average

net steady-state charge density is calculated as

$$Q_{ss} = qd \left(\frac{1}{d} \int_0^d |n - p| dx \right)$$

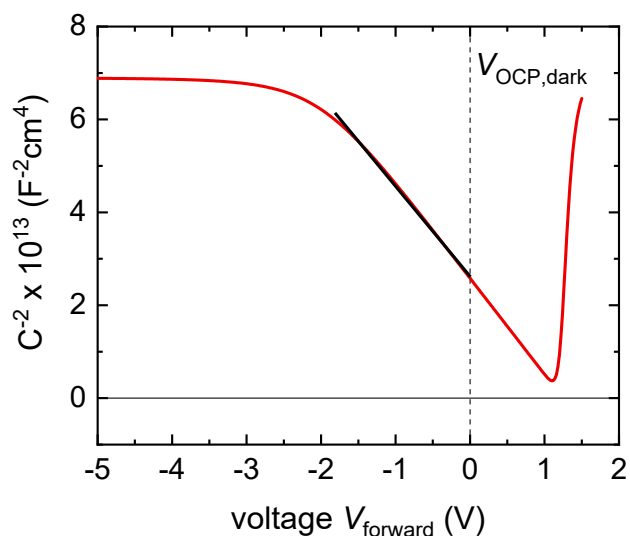


Figure S2 Simulated Mott-Schottky behaviour of a doped photoanode ($N_d = 10^{17} \text{ cm}^{-3}$) in the dark, with the same parameters as table S1. In this situation, the capacitance at equilibrium and deep reverse bias is dominated by the depletion capacitance, which means the linear Mott-Schottky region should be clearly visible at (and hence can be fitted at) deep reverse or anodic biases, as shown using the black line.

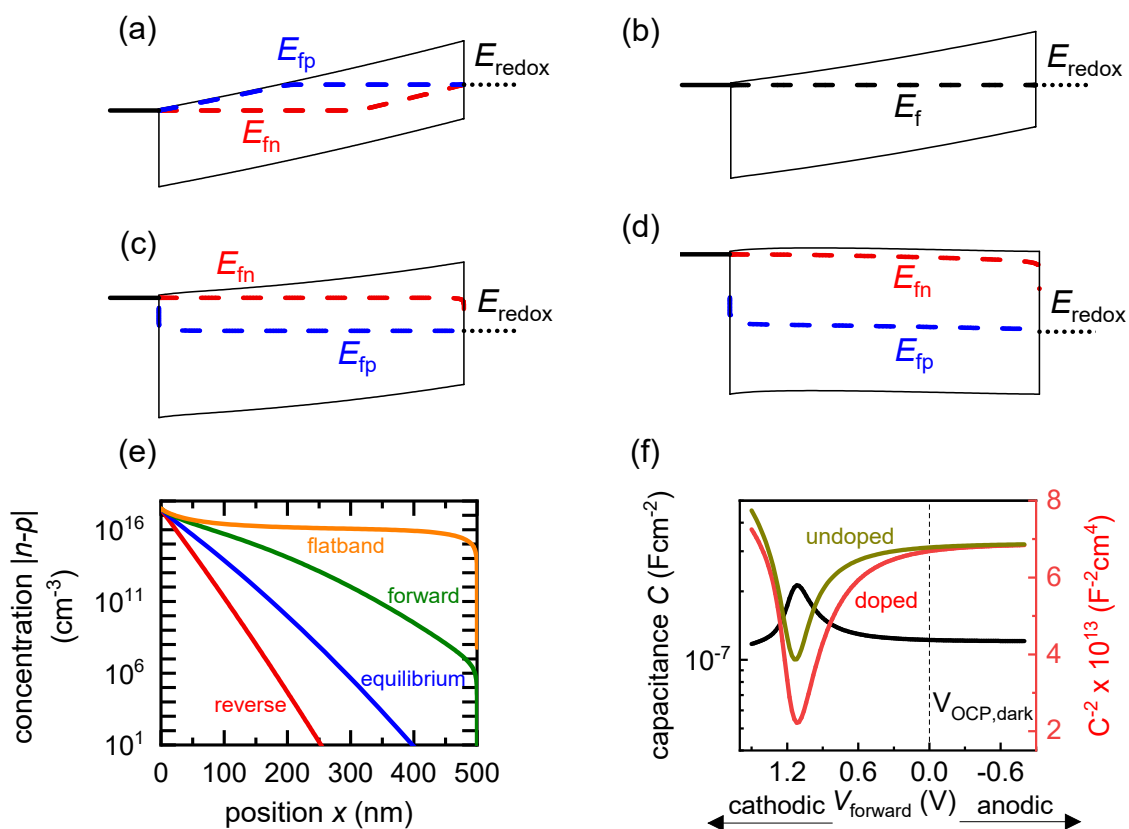


Figure S3 Simulated band diagrams of a doped photoanode ($N_d = 10^{16} \text{ cm}^{-3}$) in the dark at (a)

deep reverse bias, (b) equilibrium, (c) forward bias and (d) flatband conditions. (e) shows the corresponding total concentration $|n-p|$ as a function of position in the photoanode for the different situations in (a)-(d). (f) shows the capacitance step and corresponding Mott-Schottky plot from a simulated small-perturbation capacitance-voltage measurement (10^3 Hz). Also shown in (f) is the Mott-Schottky plot generated by an undoped (intrinsic) absorber layer. Simulation parameters are shown in Table S1. The Mott-Schottky plot due to the existence of a doping density is still very difficult to distinguish experimentally from that generated by an undoped absorber layer.

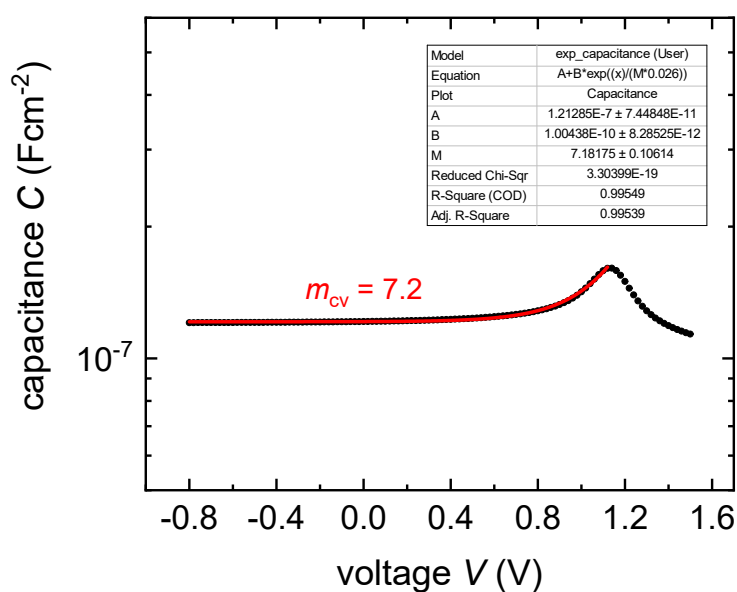


Figure S4 Fitting (red line) of the rising capacitance step generated by an undoped, intrinsic photoanode (figure 3(f) in the main text) to equation 8 in the main text. The m_{cv} factor obtained from the fit is also shown.

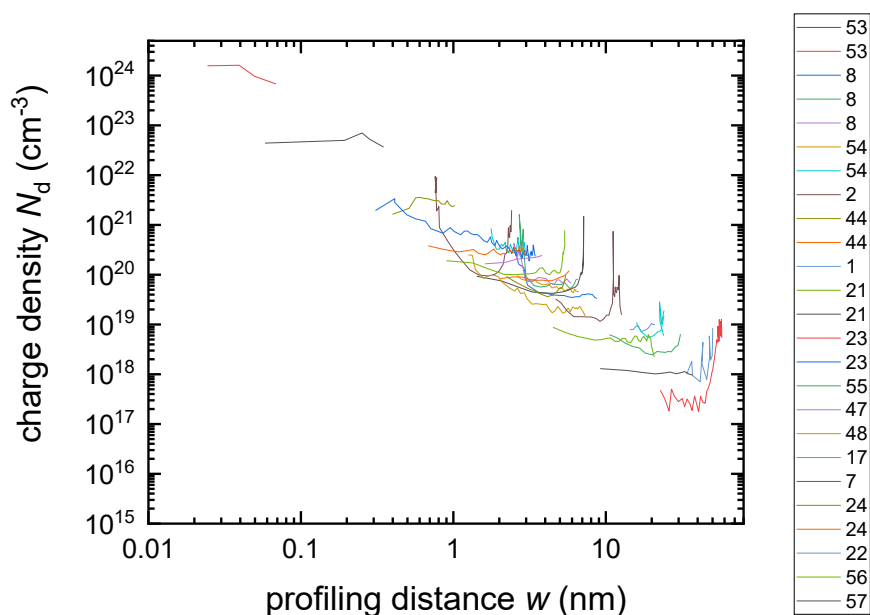


Figure S5 Calculated doping profiles of the literature data points in figures 4(b) and 4(d). A relative permittivity value of 32 for haematite, 68 for bismuth vanadate and 12.5 for indium phosphide was assumed to calculate the doping profiles. The doping densities were obtained from the plateau regions of the doping profiles. The numbers of the references in the main paper corresponding to these doping profiles are shown in the label.

References

1. M. Burgelman, P. Nollet and S. Degrave, *Thin solid films*, 2000, **361**, 527-532.
2. R. E. Schropp and M. Zeman, *Amorphous and microcrystalline silicon solar cells: modeling, materials and device technology*, Springer, 1998.
3. D. Abou-Ras, T. Kirchartz and U. Rau, *Advanced characterization techniques for thin film solar cells*, Wiley Online Library, 2011.
4. T. Kirchartz and J. Nelson, *Multiscale Modelling of Organic and Hybrid Photovoltaics*, Springer, 2013, pp. 279-324.
5. K. Sayama, A. Nomura, T. Arai, T. Sugita, R. Abe, M. Yanagida, T. Oi, Y. Iwasaki, Y. Abe and H. Sugihara, *J. Phys. Chem. B*, 2006, **110**, 11352-11360.
6. D. Zhou, L.-X. Pang, J. Guo, Z.-M. Qi, T. Shao, Q.-P. Wang, H.-D. Xie, X. Yao and C. A. Randall, *Inorg. Chem.*, 2014, **53**, 1048-1055.
7. B. J. Trzeźniewski and W. A. Smith, *J. Mater. Chem. A*, 2016, **4**, 2919-2926.
8. A. J. E. Rettie, H. C. Lee, L. G. Marshall, J.-F. Lin, C. Capan, J. Lindemuth, J. S. McCloy, J. Zhou, A. J. Bard and C. B. Mullins, *J. Am. Chem. Soc.*, 2013, **135**, 11389-11396.
9. Y. Ma, S. R. Pendlebury, A. Reynal, F. Le Formal and J. R. Durrant, *Chem. Sci.*, 2014, **5**, 2964-2973.
10. S. R. Pendlebury, M. Barroso, A. J. Cowan, K. Sivula, J. Tang, M. Grätzel, D. Klug and J. R. Durrant, *Chem. Commun.*, 2011, **47**, 716-718.
11. C. Y. Cummings, F. Marken, L. M. Peter, A. A. Tahir and K. U. Wijayantha, *Chem. Commun.*, 2012, **48**, 2027-2029.
12. L. M. Peter, *J. Solid State Electrochem.*, 2013, **17**, 315-326.